International Journal of Hydrogen Energy 106 (2025) 226–230

Contents lists available at ScienceDirect

International Journal of Hydrogen Energy

journal homepage: www.elsevier.com/locate/he

Multilayer alumina/aluminum coatings for damage-resistant hydrogen permeation barrier

Jinwoo Kim [a,1,2], Xiahui Yao [b,1], Vrindaa Somjit [a], So Yeon Kim [a,b], Ju Li [a,b,**], Bilge Yildiz [a,b,***], C. Cem Tasan [a,*]

[a] Department of Materials Science and Engineering, Massachusetts Institute of Technology, 77 Massachusetts Avenue, Cambridge, MA, 02139, United States
[b] Department of Nuclear Science and Engineering, Massachusetts Institute of Technology, 77 Massachusetts Avenue, Cambridge, MA, 02139, United States

ARTICLE INFO

Handling Editor: Dr C O Colpan

Keywords:
Hydrogen embrittlement
Hydrogen permeation barriers
Damage resistance
Multilayer coatings

ABSTRACT

Physical inhibition of hydrogen permeation into base metals using hydrogen permeation barrier coatings is a straightforward way to prevent the hydrogen embrittlement of the structural metals. We propose the multilayered coatings of alternate alumina and aluminum layers as promising hydrogen permeation barrier materials that possess extremely low H permeability as well as improved damage resistance. Electrochemical hydrogen permeation tests demonstrated that incorporating multiple layer interfaces reduces the H diffusivity of multilayer coatings (1.35×10^{-21} m^2/s in the quad-layer coating), comparable with or even lower than that of a dense single alumina coating (2.97×10^{-21} m^2/s). Furthermore, bending tests revealed that the multilayer structure also enhances the resistance of coatings to cracking and delamination. This multilayer design of hydrogen permeation barrier coatings offers an effective strategy for obtaining the combination of low hydrogen permeability and robust mechanical reliability, making them suitable for preventing hydrogen embrittlement in structural alloys.

Hydrogen embrittlement (HE) poses a significant challenge to the mechanical reliability of structural metals for hydrogen energy infrastructures and deep-sea applications. Several solutions for HE have been proposed such as (i) physical/chemical inhibitors to prevent hydrogen ingress [1], (ii) alloy design for inherent HE resistance by microstructural hydrogen traps [2] or H-induced transition of deformation mechanism [3,4], (iii) hydrogen removal from base metals by thermal [5] or electrochemical treatment [6]. Hydrogen permeation barrier (HPB) coatings, particularly those based on oxide or nitride materials, have emerged as promising solutions impeding the fundamental source of HE, hydrogen permeation into base metals. However, the practical applications of these ceramic coatings are hindered by inherent limitations in their low damage resistance and mechanical reliability.

The primary requirement for HPB coatings is an extremely low hydrogen permeability. The hydrogen permeability is the product of hydrogen solubility and diffusivity, but the diffusivity plays a more critical role in obtaining a low permeability than the solubility for most HPB candidate materials. Aluminum oxide (α-Al_2O_3) is a representative material for HPB coating. Its hydrogen diffusivity at room temperature was estimated to be 2.32×10^{-28} m^2/s by theoretical calculations [7], and 9.25×10^{-22} m^2/s by experimental measurements [8], which are approximately 10 orders of magnitude lower than that of ferritic stainless steels (10^{-11}-10^{-12} m^2/s [9,10]). Aluminum metal has a relatively low hydrogen diffusivity (1.51×10^{-14} m^2/s [11]) among pure metals but it is not low enough for long-term HPB, compared to that of ceramic compounds such as α-Al_2O_3.

In this study, we design a multilayer coating which aims to obtain

* Corresponding author.
** Corresponding author. Department of Materials Science and Engineering, Massachusetts Institute of Technology, 77 Massachusetts Avenue, Cambridge, MA, 02139, United States.
*** Corresponding author. Department of Materials Science and Engineering, Massachusetts Institute of Technology, 77 Massachusetts Avenue, Cambridge, MA, 02139, United States.
E-mail addresses: liju@mit.edu (J. Li), byildiz@mit.edu (B. Yildiz), tasan@mit.edu (C.C. Tasan).
[1] These authors contributed equally to this work.
[2] Present address: Center for Hydrogen Energy Materials, Korea Institute of Science and Technology, 5 Hwarang-ro 14-gil, Seongbuk-gu, Seoul 02792, Republic of Korea.

https://doi.org/10.1016/j.ijhydene.2025.01.300
Received 25 September 2024; Received in revised form 29 November 2024; Accepted 19 January 2025
Available online 3 February 2025
0360-3199/© 2025 Hydrogen Energy Publications LLC. Published by Elsevier Ltd. All rights are reserved, including those for text and data mining, AI training, and similar technologies.

excellent HPB performance (i.e., extremely low hydrogen diffusivity) as well as robust mechanical properties [12–15]. Previous research efforts on multilayer HPB coatings have widely focused on ceramic/ceramic multilayers, such as Al_2O_3/Cr_2O_3 [16,17], Er_2O_3/SiC [18], Y_2O_3/Cr_2O_3 [19], Er_2O_3/ZrO_2 [20], for H-isotope permeation barriers in high-temperature fusion reactor applications. Here, we propose a multilayered structure comprising aluminum metal (Al) and aluminum oxide (AO) for preventing near-room temperature HE in structural alloys, guided by theoretical insights derived from our previous study [21] using density-functional theory (DFT) and Grand Canonical Monte Carlo (GCMC) simulations. The findings revealed the possibility that the interface between Al and AO forms superabundant metal vacancies that can trap multiple hydrogen atoms [21], which is expected to hinder hydrogen diffusion across the interface.

Al and AO depositions were carried out through RF magnetron sputtering using the AJA Model ATC Orion 5 system, on commercial 430 stainless steel substrates with a thickness of 300 μm. Two Al sputtering targets (99.999%, Kurt J. Lesker) were employed, and a pre-sputtering phase lasting 5 min preceded the deposition process to remove the oxide layer from the sputtering targets and residual oxygen in the sputtering chamber. Throughout the process, the base pressure was initially reduced to 1×10^{-3} mTorr before introducing the gas. It was then maintained at 30 mTorr during ignition and subsequently reduced to 3 mTorr during deposition. For Al deposition, an argon (Ar) flow rate of 12 sccm was utilized with a power setting of 100 W. The deposition rate was measured to be ~1 Å/s by a quartz crystal monitor. For AO deposition by reactive sputtering, both Ar and oxygen (O_2) were introduced into the chamber, with flow rates of 10 sccm and 2 sccm, respectively, following the method described in Ref. [22]. For multilayers, the chamber was pumped down again to reach a base pressure of 1×10^{-3} mTorr, and an additional pre-sputtering step was performed before depositing each Al layer. The power was set to 150 W, yielding a deposition rate of ~1.3–1.4 Å/s. Throughout the process, the base pressure was maintained at 30 mTorr during ignition and reduced to 3 mTorr during deposition. The duration of deposition was determined based on the desired thickness and the measured deposition rate. In order to perform the electrochemical H permeation tests, a conductive Cr layer of 100 nm thickness was deposited on the top of AO/Al coatings using a Cr sputtering target (99.95 %, Kurt J. Lesker). For Cr deposition, an Ar flow rate of 12 sccm was used with a power of 140 W, which yielded a deposition rate of 0.95 Å/s"

Electrochemical H permeation tests were performed using a modified Devanathan-Stachurski H-permeation cell according to ASTM G148-97 [23]. The coated specimens were placed between the two half cells, H-charging side and H-detection side. Pt wires were used as counter electrodes for both half cells. For the H-charging side cell, a 3 % NaCl aqueous solution with 3 g/L NH_4SCN was used as the electrolyte, and a constant current density of 0.1 mA/cm^2 was applied. For the H-detection side cell, a 0.1 M NaOH aqueous solution was used as the electrolyte, and a constant potential of +0.3 V versus Hg/HgO reference electrode was applied. The effective H diffusivity, D_{eff}, was determined by the breakthrough method [23], $D_{eff} = L^2/(15.3\ t_b)$. L is the thickness of the specimen and t_b is the breakthrough time (elapsed time measured extrapolating the linear portion of the rising permeation current (J) transient to $J = 0$). For calculating the H diffusivity of a coating, only the thickness of the coating was considered as L, since the permeation time for the bare substrate was negligibly small compared to that for the coated specimens (See Fig. 1(a)).

Bending tests of the coated specimens were conducted to evaluate the deformation behavior and the capability for retention of the HPB performance of coatings. In order to obtain a target strain at the top surface (at the coating layers), $\varepsilon_{surf} = L/(2\ r + L)$, the coated specimens were pressed on a plate with a defined radius, r, as shown in Fig. 3(a). The specimens were unbent to a flat shape before the H permeation tests and microscopic observations. The surface morphology and the cross-section microstructure were observed by a scanning electron microscope (SEM, Tescan MIRA3) equipped with an Everhart-Thornley (E-T) type secondary electron (SE) detector and an In-beam type SE detector. A focused ion beam (FEI Helios Nanolab 600) system was used to prepare the specimen for cross-section observation.

We first examined the effect of the number of layers on the H diffusivity of coatings. Fig. 1 shows the electrochemical H permeation test results of an uncoated 430 stainless steel and coated specimens with different numbers of alternate layers of AO and Al. The total thickness of coating ($t_{c,total}$) for all coated specimens is 100 nm, and the thickness of individual layers in a multilayer coating was controlled to be equal. The top layer is AO for all coatings. For example, the quad-layer coating has the layer order of AO/Al/AO/Al/substrate with an individual layer thickness of 25 nm. The onset of apparent rise in the H-oxidation current curves in Fig. 1(a) reflects the hydrogen permeation fully across the specimen. The effective H diffusivity of the specimens was evaluated from the H-permeation curves using the breakthrough time (t_b) [23] as shown in Fig. 1(b). The single layer (100% AO) coated specimen shows a D_{eff} value close to the previously reported value for AO [8]. Based on the rule of mixture (without considering effects of interfaces), the effective H diffusivity of multilayer coatings with the equivalent portions of Al and AO can be estimated by $D_{eff} \approx 4D_{AO}$ (see Supplementary Materials), given the relatively high H diffusivity of Al, ~10^{-14} m^2/s [11]). The double layer coated specimen exhibits a D_{eff}, value slightly higher than the estimation. Interestingly, from the double to quad layer coatings, D_{eff} decreases with increasing the number of layers. The quad layer coating has an even lower H diffusivity than the single AO coating despite its large Al portion (50%). After heat treatment at 673 K for 2 h the H diffusivity in the quad layer coating was able to be reduced further, which may indicate densification of individual layers or enhancement of interface adhesion including the formation of a thicker interdiffusion

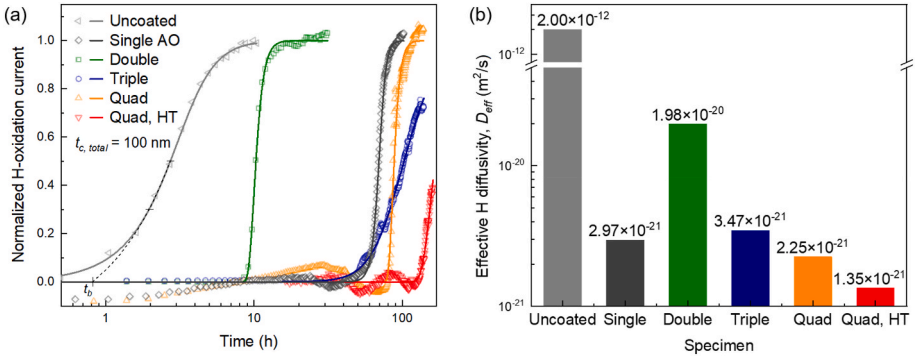

Fig. 1. (a) Hydrogen permeation curves obtained from an uncoated substrate and coated specimens with different numbers of layers. The data points were fitted with the logistic function (solid lines), and the H-oxidation current (y-axis) were normalized by the saturation current obtained from the fitting curves. (b) Effective hydrogen diffusivity (D_{eff}) of specimens determined by the breakthrough method [23].

layer at the interface by the heat treatment. The overall permeation test results in Fig. 1 indicate that adding the AO/Al interfaces into the coatings can improve their H permeation barrier performance.

Interfaces such as grain boundaries and phase boundaries are known to be moderate-to-strong hydrogen trapping sites [2,24]. Especially, the AO/Al interface can trap hydrogen atoms strongly. This is due to the high segregation energies of hydrogen towards the interface as calculated using density functional theory in our previous study [21]. The segregation energy of hydrogen to the interface is 3.2 eV (from the oxide side) and 0.39 eV (from the aluminum side), indicating a strong preference for hydrogen to reside at the interface compared to the bulk materials. In the study [21], we also carried out ab initio Monte Carlo (MC) simulations with hydrogen initially placed at random places in the AO/Al supercell, including in the AO bulk and Al bulk, and found that hydrogen atoms were driven towards the interface as the MC run proceeded (Fig. 2). Thus, hydrogen prefers to remain trapped at the interface by passivating the under-coordinated Al atoms due to favorable thermodynamics. Additionally, hydrogen diffusion through bulk AO and Al is also slow (activation energy for hydrogen diffusion in AO is ~2.25 eV [25], and in Al is 0.46 eV [26]). Thus, once trapped at the interface, both thermodynamics and kinetics would likely make it unfavorable for hydrogen to escape the interface. These properties make our multilayer interface combination favorable and could provide an indication why increasing the number of layers lowers hydrogen permeation.

We compared the single AO coating and the quad layer coating in terms of the capability for retention of HPB performance after deformation, using bending tests. Fig. 3(a) presents the H permeation curves for both coatings after bending. The single AO-coated specimen after bending to $\varepsilon_{surf} = 0.5$ % shows the rise of H-permeation current with the onset ~1 h, which approaches that of the uncoated substrate. This represents that the bending deformation induces critical damage to the HPB performance of AO coating. On the other hand, the quad layer coating after bending to $\varepsilon_{surf} = 0.5$ % shows no significant rise in H-permeation current for the tested time range (~12 h), and it exhibits less H-permeation even after bending to $\varepsilon_{surf} = 1.0$ %, compared to the 0.5 %-bent single AO coated specimen. This demonstrates that the quad layer coating is able to retain its HPB performance significantly better than the single AO coating.

The reduction of HPB performance could be associated with cracking of coatings by bending deformation. Cracking of coatings also leads to the crevice formation on the surface and accelerates local corrosion, particularly in aqueous environments such as in marine applications, so cracking resistance is a critical factor for reliable HPB coatings. We observed the coating surfaces using SEM after bending to different levels of ε_{surf}, as presented in Fig. 4. The single AO coatings do not have any crack in the surface up to $\varepsilon_{surf} = 0.3$ % (Fig. 4(a)), while a few cracks are observed on the surface after bending to $\varepsilon_{surf} = 0.4$ % (Fig. 4(b)) and $\varepsilon_{surf} = 0.5$ % (Fig. 4(c)). The onset ε_{surf} for surface cracking in the quad layer

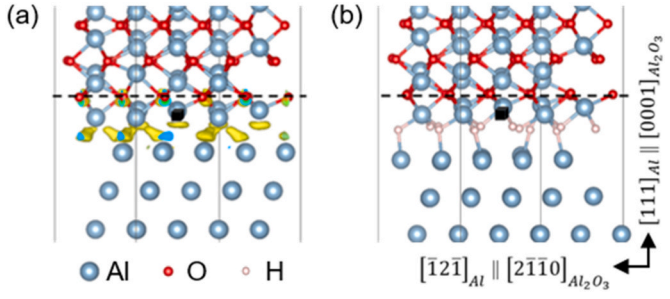

Fig. 2. (a) Partial charge density (yellow regions) at the interfaces explored by ab initio MC and (b) equilibrium interface structures obtained for MC runs with 12 H atoms in the system. Reproduced from Ref. [21]. (For interpretation of the references to colour in this figure legend, the reader is referred to the Web version of this article.)

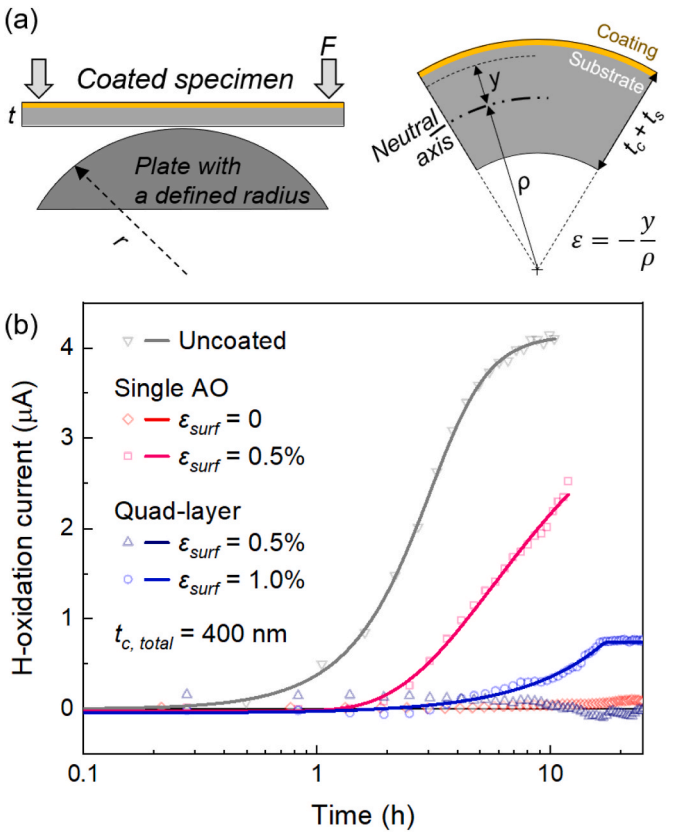

Fig. 3. (a) Schematic diagrams describing the bending test method used in this study and the calculation of surface strain applied to the coatings. (b) Hydrogen permeation curves obtained from coated specimens with a single layer AO coating and a quad-layer coating (AO/Al/AO/Al) after bending deformation. The total thickness of coating ($t_{c,total}$) for the both coated specimens is 400 nm.

coating is higher than in the single AO coating. No cracks are observed on the surface of the quad layer coating up to 0.6 % (Fig. 4(d)), and multiple cracks are detected after bending to $\varepsilon_{surf} = 0.7$ % (Fig. 4(e)) and $\varepsilon_{surf} = 0.8$ % (Fig. 4(f)). The number of surface cracks per area collected from the SEM images is plotted depending on ε_{surf} in Fig. 4(g). These observations correspond well with the H permeation tests of bent specimens. The higher onset strain for crack initiation enables the quad layer coating to retain its HPB performance against deformation.

The cross-section SE images of a bent quad layer specimen ($\varepsilon_{surf} = 1.0$ %) in Fig. 5(a and b) present that the major crack has a deflection at an Al/AO interface in the middle and the first Al layer on the substrate has elongated morphology across the crack that is the indication of plasticity. Both could contribute to the improved damage resistance of the coating, where the former contributes to extrinsic toughening and the latter to intrinsic toughening [27]. The minor cracks observed in the top AO layer represent that the initial stage of crack propagation is blocked at the AO/Al interface (Fig. 5(c)), which also supports the extrinsic toughening of the multilayer coating by the interface. These components enhancing the damage resistance are supposed to also result in a larger number of finely dispersed surface cracks in the quad layer coating (Fig. 4(e) and (f)) compared to the single AO coating.

We also compared the resistance against delamination for both coatings. After bending to a large strain of $\varepsilon_{surf} = 1.0$ %, the single AO coated specimen shows obvious delamination of coatings as shown in the SEM images of Fig. 5(d). Delaminated tips of the AO coating are observed as marked with the red arrows in the E-T SE image. Beyond the tips, the dark contrast regions in the In-beam SE image represent the coating areas that lost the adhesion on the substrate. On the other hand, the quad layer coating presents no clear indication of delamination in

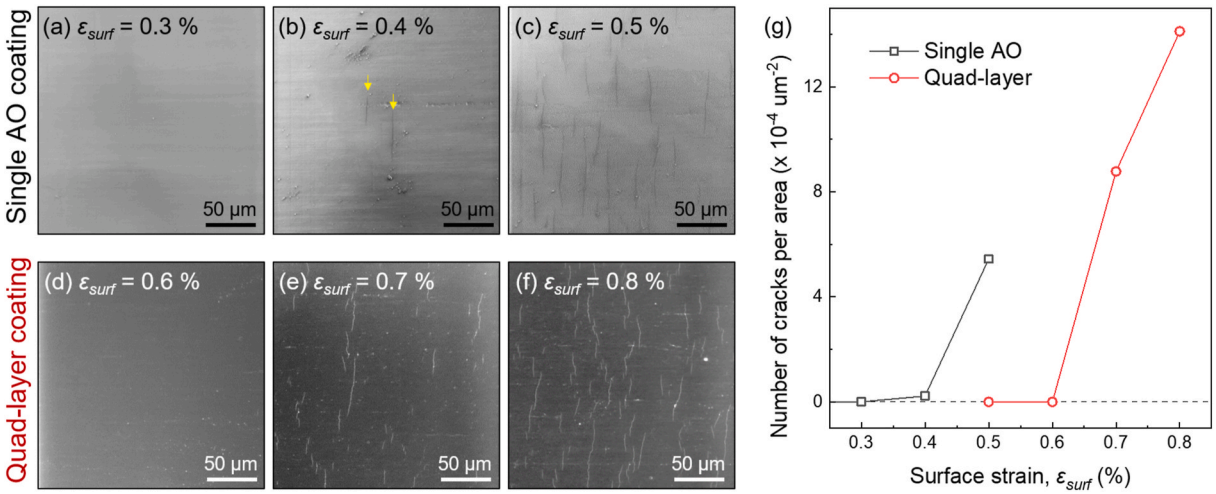

Fig. 4. (a–c) In-beam SE images of single AO-coated specimens after bending to different surface strain (ε_{surf}): (a) 0.3 %, (b) 0.4 %, and (c) 0.5 %. (d–f) In-beam SE images of quad layer-coated specimens after bending to ε_{surf} = (a) 0.6 %, (b) 0.7 %, and (c) 0.8 %, respectively. (g) The number of cracks per area depending on ε_{surf} in the two coatings, obtained from the SEM image analysis.

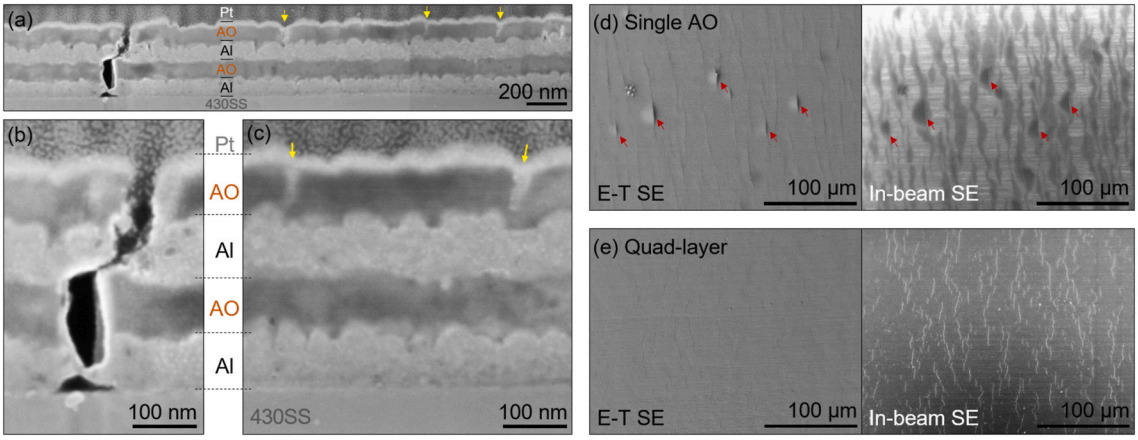

Fig. 5. (a–c) Cross-section in-beam images of the quad-layer coating prepared by focused ion beam. (a) Low-magnification image of the observed area showing multiple cracks. The minor cracks in the top AO layer are highlighted with yellow allows. (b) A major crack penetrating the whole coating. The Al metal layers show deflection of the crack path and necking-like plastic deformation. (c) Minor cracks arrested in the top AO layer. (d,e) E-T SE (left) and in-beam SE (right) surface images of the coated specimens after bending to ε_{surf} = 1.0 %. (d) single AO coating. (e) quad-layer coating. (For interpretation of the references to colour in this figure legend, the reader is referred to the Web version of this article.)

both SE images in Fig. 5(e). The cross-section SE images in Fig. 5(d and e) also suggest the limited delamination of the bent quad layer coating around a crack. This could be attributed to the presence of an Al layer between the AO layer and the substrate, which acts as a buffer layer enhancing the adhesion between the oxide layer and the steel substrate.

In the multilayer design for H permeation barrier coatings proposed in this work, thinner Al layers would be beneficial in terms of lowering the overall effective H diffusivity, but may reduce mechanical damage resistance, the other advantage of the multilayer structure. Exploring the influence of layer thickness ratio between AO and Al would be the next step for optimizing the multilayer structure to balance H permeation barrier performance and mechanical stability. In addition, a novel large-area coating technique that can form dense layers is essential for expanding applicability of the multilayer coatings. Sputtering techniques such as the RF magnetron sputtering used in this work may not be suitable for large-area applications. In contrast, coatings prepared by sol-gel based methods which have a large-area applicability do not form dense AO layers suitable for excellent H permeation barriers (see Supplementary Materials).

In summary, the multilayer structure of alternate AO and Al layers provides the superior HPB performance and the resistance against cracking and delamination. We confirmed that increasing the number of alternate Al/AO layers can decrease the effective hydrogen diffusivity to the values much lower than that estimated from the rule of mixture. In other words, increasing the number of Al/AO interfaces can enhance the performance of HPB coatings. The interface between AO and Al layers also contributes to the enhancement of their damage resistance. Additionally, the Al layer between the AO layer and the steel substrate acts as a buffer layer that improves coating adhesion and resistance to delamination. As demonstrated in this work, multilayering oxide and metal layers could provide an effective strategy to secure the low H permeability and mechanical reliability simultaneously for HPB coatings to prevent HE of advanced structural alloys. Some aspects should be investigated in further studies to broaden the applicability, such as (i) possible damages at the interface by excessive H segregation [21], (ii) high temperature HPB performance of which potentiality was hinted by the heat-treated quad layer coating (Fig. 1), and (iii) deposition methods for large-area coatings.

CRediT authorship contribution statement

Jinwoo Kim: Writing – review & editing, Writing – original draft, Methodology, Investigation, Formal analysis, Data curation. **Xiahui Yao:** Writing – review & editing, Methodology, Investigation, Formal analysis, Data curation. **Vrindaa Somjit:** Writing – review & editing, Methodology, Investigation, Formal analysis. **So Yeon Kim:** Writing – review & editing, Investigation, Formal analysis, Data curation. **Ju Li:** Writing – review & editing, Supervision, Resources, Methodology, Funding acquisition, Conceptualization. **Bilge Yildiz:** Writing – review & editing, Supervision, Software, Resources, Project administration, Funding acquisition, Conceptualization. **C. Cem Tasan:** Writing – review & editing, Supervision, Resources, Project administration, Methodology, Conceptualization.

CRediT authorship contribution statement

Jinwoo Kim: Writing – review & editing, Writing – original draft, Methodology, Investigation, Formal analysis, Data curation. **Xiahui Yao:** Writing – review & editing, Methodology, Investigation, Formal analysis, Data curation. **Vrindaa Somjit:** Writing – review & editing, Methodology, Investigation, Formal analysis. **So Yeon Kim:** Writing – review & editing, Investigation, Formal analysis, Data curation. **Ju Li:** Writing – review & editing, Supervision, Resources, Methodology, Funding acquisition, Conceptualization. **Bilge Yildiz:** Writing – review & editing, Supervision, Software, Resources, Project administration, Funding acquisition, Conceptualization. **C. Cem Tasan:** Writing – review & editing, Supervision, Resources, Project administration, Methodology, Conceptualization.

Declaration of competing interest

The authors declare that they have no known competing financial interests or personal relationships that could have appeared to influence the work reported in this paper.

Acknowledgements

The authors gratefully acknowledge financial support by Exelon Corporation - Agreement Effective 4/1/16.

Appendix A. Supplementary data

Supplementary data to this article can be found online at https://doi.org/10.1016/j.ijhydene.2025.01.300.

References

[1] Holbrook JH, Cialone HJ, Collings EW, Drauglis EJ, Scott PM, Mayfield ME. 5 - control of hydrogen embrittlement of metals by chemical inhibitors and coatings. In: Gaseous hydrogen embrittlement of materials in energy technologies. Woodhead Publishing; 2012. p. 129–53. https://doi.org/10.1533/9780857095374.1.129.

[2] Bhadeshia HKDH. Prevention of hydrogen embrittlement in steels. ISIJ Int 2016;56:24–36. https://doi.org/10.2355/isijinternational.ISIJINT-2015-430.

[3] Luo H, Li Z, Raabe D. Hydrogen enhances strength and ductility of an equiatomic high-entropy alloy. Sci Rep 2017;7:9892. https://doi.org/10.1038/s41598-017-10774-4.

[4] Luo H, Lu W, Fang X, Ponge D, Li Z, Raabe D. Beating hydrogen with its own weapon: nano-twin gradients enhance embrittlement resistance of a high-entropy alloy. Mater Today 2018;21:1003–9. https://doi.org/10.1016/J.MATTOD.2018.07.015.

[5] Yi K, Ma R, Xiang S, Liu X, Liu C, Zhang X, Fu Y. Eliminating reversible hydrogen embrittlement in high-strength martensitic steel by an electric current pulse. Int J Hydrogen Energy 2022;47:17045–55. https://doi.org/10.1016/j.ijhydene.2022.03.169.

[6] Kim J, Yao X, Kong D, Li J, Yildiz B, Tasan CC. Electrochemical pumping: an alternative solution for hydrogen embrittlement. Appl Mater Today 2022;29:101627. https://doi.org/10.1016/j.apmt.2022.101627.

[7] Belonoshko AB, Rosengren A, Dong Q, Hultquist G, Leygraf C. First-principles study of hydrogen diffusion in α-Al2O3 and liquid alumina. Phys Rev B 2004;69:24302. https://doi.org/10.1103/PhysRevB.69.024302.

[8] Serra E, Calza Bini A, Cosoli G, Pilloni L. Hydrogen permeation measurements on alumina. J Am Ceram Soc 2005;88:15–8. https://doi.org/10.1111/j.1551-2916.2004.00003.x.

[9] San Marchi C, Zelinski JA. Technical reference on hydrogen compatibility of materials high-alloy ferritic steels: ferritic stainless steels (code 1500). https://www.sandia.gov/matlsTechRef/; 2012.

[10] Yen SK, Huang IB. Hydrogen permeation tests in laminates: application to grain/grain boundary of AISI 430 stainless steel. Corrosion 2003;59.

[11] Saitoh H, Iijima Y, Tanaka H. Hydrogen diffusivity in aluminium measured by a glow discharge permeation method. Acta Metall Mater 1994;42:2493–8. https://doi.org/10.1016/0956-7151(94)90329-8.

[12] Putz B, Edwards TEJ, Huszar E, Pethö L, Kreiml P, Cordill MJ, Thiaudiere D, Chiroli S, Zighem F, Faurie D, Renault P-O, Michler J. In situ fragmentation of Al/Al2O3 multilayers on flexible substrates in biaxial tension. Mater Des 2023;232:112081. https://doi.org/10.1016/j.matdes.2023.112081.

[13] Putz B, Edwards TEJ, Huszar E, Gruber PA, Gradwohl K-P, Kreiml P, Többens DM, Michler J. Electromechanical behavior of Al/Al2O3 multilayers on flexible substrates: insights from in situ film stress and resistance measurements. Adv Eng Mater 2023;25:2200951. https://doi.org/10.1002/adem.202200951.

[14] Edwards TEJ, Xie T, Maria della Ventura N, Casari D, Guerra C, Huszár E, Maeder X, Schwiedrzik JJ, Utke I, Pethö L, Michler J. On the thinnest Al2O3 interlayers in Al-based nanolaminates to enhance strength, and the role of constraint. Acta Mater 2022;240:118345. https://doi.org/10.1016/j.actamat.2022.118345.

[15] Xie T, Edwards TEJ, della Ventura NM, Casari D, Huszár E, Fu L, Zhou L, Maeder X, Schwiedrzik JJ, Utke I, Michler J, Pethö L. Synthesis of model Al-Al2O3 multilayer systems with monolayer oxide thickness control by circumventing native oxidation. Thin Solid Films 2020;711:138287. https://doi.org/10.1016/j.tsf.2020.138287.

[16] He D, Lei Y, Zhang C, Li S, Liu X, Zhang H, Lv Q, Wu Y, Jiang L. Deuterium permeation of Al2O3/Cr2O3 composite film on 316L stainless steel. Int J Hydrogen Energy 2015;40:2899–903. https://doi.org/10.1016/j.ijhydene.2014.12.058.

[17] Wang L, Wu YY, Luo XF, Ning ZE, Wang JH, Yang JJ, Feng YJ, Liao JL, Yang YY, Feng KM, Liu N, Gong M. Effects of Ar/O2 ratio on preparation and properties of multilayer Cr2O3/α-Al2O3 tritium permeation barrier. Surf Coat Technol 2018;339:132–8. https://doi.org/10.1016/j.surfcoat.2018.02.021.

[18] Zhu S, Wu Y, Liu T, Wang X, Yan J, Yin A. Interface structure and deuterium permeation properties of Er2O3/SiC multilayer film prepared by RF magnetron sputtering. Int J Hydrogen Energy 2015;40:5701–6. https://doi.org/10.1016/j.ijhydene.2015.02.128.

[19] Wu Y, He D, Li S, Liu X, Wang S, Jiang L. Deuterium permeation properties of Y2O3/Cr2O3 composite coating prepared by MOCVD on 316L stainless steel. Int J Hydrogen Energy 2016;41:7425–30. https://doi.org/10.1016/j.ijhydene.2016.03.132.

[20] Mochizuki J, Horikoshi S, Fujita H, Matsunaga M, Hishinuma Y, Oya Y, Chikada T. Preparation and characterization of Er2O3-ZrO2 multi-layer coating for tritium permeation barrier by metal organic decomposition. Fusion Eng Des 2018;136:219–22. https://doi.org/10.1016/j.fusengdes.2018.01.059.

[21] Somjit V, Yildiz B. Charge trapping at Al/Al2O3 interface facilitates hydrogen-induced superabundant metal vacancy formation. Phys Rev Mater 2023;7:L072001. https://doi.org/10.1103/PhysRevMaterials.7.L072001.

[22] Chiba Y, Abe Y, Kawamura M, Sasaki K. Formation process of Al2O3 thin film by reactive sputtering. Vacuum 2008;83:483–5. https://doi.org/10.1016/j.vacuum.2008.04.012.

[23] Standard Practice for Evaluation of Hydrogen Uptake, Permeation, and Transport in Metals by an Electrochemical Technique, n.d. https://doi.org/10.1520/G0148-97R18.

[24] Koyama M, Rohwerder M, Tasan CC, Bashir A, Akiyama E, Takai K, Raabe D, Tsuzaki K. Recent progress in microstructural hydrogen mapping in steels: quantification, kinetic analysis, and multi-scale characterisation. Mater Sci Technol 2017;33:1481–96. https://doi.org/10.1080/02670836.2017.1299276.

[25] Fowler JD, Chandra D, Elleman TS, Payne AW, Verghese K. Tritium diffusion in Al2O3 and BeO. J Am Ceram Soc 1977;60:155–61. https://doi.org/10.1111/j.1151-2916.1977.tb15493.x.

[26] Ichimura M, Sasajima Y, Imabayashi M. Grain boundary effect on diffusion of hydrogen in pure aluminum. Mater Trans, JIM 1991;32:1109–14. https://doi.org/10.2320/matertrans1989.32.1109.

[27] Ritchie RO. Toughening materials: enhancing resistance to fracture. Phil Trans Math Phys Eng Sci 2021;379:20200437. https://doi.org/10.1098/rsta.2020.0437.